Colloid Polym Sci (2008) 286:805–812
DOI 10.1007/s00396-008-1873-3

SHORT COMMUNICATION

Direct imaging of temperature-sensitive core-shell latexes by cryogenic transmission electron microscopy

Jérôme J. Crassous · Alexander Wittemann · Miriam Siebenbürger · Marc Schrinner · Markus Drechsler · Matthias Ballauff

Received: 22 February 2008 / Revised: 2 April 2008 / Accepted: 7 April 2008 / Published online: 4 May 2008

Abstract We present a comprehensive investigation of the volume transition in thermosensitive core-shell particles. The particles consist of a solid core of poly (styrene) (radius: 52 nm) onto which a network of crosslinked poly(*N*-isopropylacrylamide) (PNIPAM) is affixed. The degree of crosslinking of the PNIPAM shell effected by the crosslinker *N*,*N*′-methylenebisacrylamide was varied between 1.25 and 5 mol%. Immersed in water, the shell of these particles is swollen at low temperatures. Raising the temperature above 32°C leads to a volume transition within the shell. Cryogenic transmission electron microscopy (Cryo-TEM) and dynamic light scattering (DLS) have been used to investigate the structure and swelling of the particles. The Cryo-TEM micrographs directly show inhomogeneities of the network. Moreover, a buckling of the shell from the core particle is evident. This buckling increases with decreasing degree of crosslinking. A comparison of the overall size of the particles determined by DLS and Cryo-TEM demonstrates that the hydrodynamic radius provides a valid measure for the size of the particles. The phase transition within the network measured by DLS can be described by the Flory–Rehner theory. It is shown that this model captures the main features of the volume transition within the core-shell particles including the dependence of the phase transition on the degree of crosslinking. All dispersions crystallize at volume fractions above 0.5. The resulting phase diagram is identical to the phase behavior of hard spheres within the limits of error. This demonstrates that the core-shell microgels can be treated as hard spheres up to volume fractions of at least 0.55.

Keywords Direct imaging · Temperature-sensitive core-shell latex · Cryogenic transmission electron microscopy · Flory-Rehner theory · Buckling · Poly(N-Isopropylacrylamide) microgels

J. J. Crassous · A. Wittemann · M. Siebenbürger · M. Schrinner · M. Ballauff (✉)
Physikalische Chemie I, University of Bayreuth, 95440 Bayreuth, Germany
e-mail: matthias.ballauff@uni-bayreuth.de

M. Drechsler
Makromolekulare Chemie II, University of Bayreuth, 95440 Bayreuth, Germany

1 Introduction

Environmentally sensitive microgels have attracted considerable interest due to their ability to swell and deswell in response to external stimuli such as temperature, pH, or light radiation [1–3]. A great number of possible applications have been discussed for these systems. A comprehensive review on the applications was given by Nayak and Lyon [4]. On the other hand, colloidal dispersions of microgels may serve as model systems for fundamental studies on the nature of liquids, solids, and glasses [5, 6]. Microgels of poly (*N*-isopropylacrylamide) (PNIPAM) crosslinked by *N*,*N*′-methylenebisacrylamide (BIS) have been of particular interest. The temperature of the volume transition is located at 32°C in aqueous solution, which makes them suitable candidates for possible medical applications, such as controlled release systems [7, 8]. Other applications include, e.g., the use of such systems as carriers for metallic nanoparticles in catalysis [9, 10].

The volume transition in macroscopic networks has been studied extensively by T. Tanaka and others

[11–14]. A thermodynamic analysis of the transition can be done in terms of the classical Flory–Rehner theory [15–19]. Hence, the volume transition in macroscopic gels seems to be rather well understood. For details, the reader is deferred to the review of Shibayama [14]. Microgels with dimensions in the colloidal domain have been the subject of a large number of experimental studies in recent years. The investigations range from measurements of the macroscopic properties, such as turbidity [20, 21], high-sensitive scanning microcalorimetry [21–23], and rheology [24, 25], to experiments probing molecular interactions such as nuclear magnetic resonance [22, 26], light scattering [15, 21, 22, 24–28], and small-angle X-ray and neutron scattering [15, 28–33]. Compared to macroscopic gels, the degree of understanding of microgels is much less advanced, however.

Here we wish to present a comprehensive study of thermosensitive core-shell particles in aqueous solution. Figure 1 displays the overall structure and the volume transition of the core-shell particles in a schematic fashion: Immersed in water, the PNIPAM-shell of the particles is swollen at low temperature. However, raising the temperature in the system above 32°C leads to a volume transition in which the network shrinks by expelling water.

These particles have been synthesized by us [31–34] and by others [22, 27, 28, 34]. They have been used as model systems for the study of the flow behavior of concentrated suspensions [6, 35, 36]. The results obtained so far provide an excellent test for the mode-coupling theory of the dynamics of dense colloidal systems [37–39]. A further point commanding attention is the crystallization of these particles. A previous study has revealed that the resulting phase diagram can be directly mapped onto the phase diagram of hard spheres [6]. Given the fact that the shells of these particles consist of a compressible network, this point is certainly in need of further elucidation.

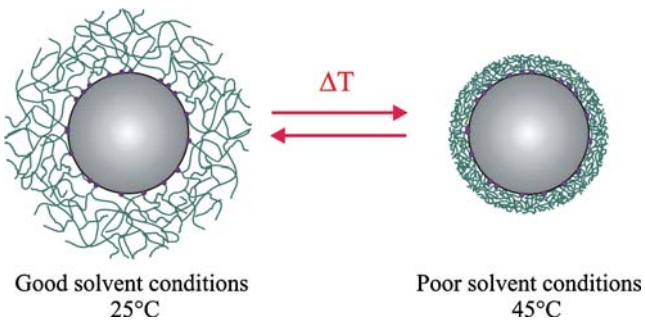

Fig. 1 Schematic representation of the volume transition in core-shell micronetworks: The polymer chains are affixed to the surface of the core

Recently, we have demonstrated that cryogenic transmission electron microscopy (Cryo-TEM) is highly suited to studying these core-shell particles in situ [9, 10, 34, 40]. Cryo-TEM allows us to visualize the particles directly in the aqueous phase by shock-freezing of a suspension of the particles. However, this novel technique has not yet been applied for a systematic study of core-shell particles differing with regard to the degree of crosslinking. In this paper, we therefore present a systematic study of core-shell microgels differing in the degree of crosslinking. Moreover, the swelling of the network is modeled in terms of the Flory–Rehner theory. Special attention is paid to the interplay of the degree of crosslinking of the particles and the phase behavior at high-volume fractions.

2 Experimental

N-Isopropylacrylamide (NIPA; Aldrich), BIS (Fluka), sodium dodecyl sulfate (Fluka), and potassium peroxodisulfate (Fluka) were used as received. Styrene (BASF) was washed with KOH solution and distilled prior to use. Water was purified using reverse osmosis (MilliRO; Millipore) and ion exchange (MilliQ; Millipore). The core-shell-type PS-NIPA particles were synthesized, purified, and characterized as described recently [31].

Cryo-TEM was done as described recently [40]. Dynamic light scattering (DLS) was done using a Peters ALV 800 light scattering goniometer. The temperature was controlled with an accuracy of 0.1°C.

3 Theoretical background

The macroscopic state of a homogeneous neutral gel is described within the classical Flory–Rehner theory. Here, we follow the exposition of this model given in [15]. Hence, it suffices to delineate the main steps.

The net osmotic pressure within the gel is given by

$$\Pi = \frac{k_b}{T}\left\{ -\phi - \ln(1-\phi) - \chi\phi^2 + \frac{\phi_0}{N_{\mathrm{Gel}}}\left[\frac{1}{2}\left(\frac{\phi}{\phi_0}\right) - \left(\frac{\phi}{\phi_0}\right)^{\frac{1}{3}}\right]\right\} \quad (1)$$

where k_B is the Boltzmann constant, χ is the Flory interaction parameter, ϕ_0 is the polymer volume fraction at a reference state, and N_{gel} is the average degree of polymerization of the polymer chain between two crosslinking points. For systems undergoing isotropic swelling, the swelling of the microgel can be described

as the ratio of the average polymer volume fraction ϕ and the average polymer volume fraction ϕ_0 in the collapsed state

$$\frac{\phi}{\phi_0} = \left[\frac{{R_{H,0}}^3 - {R_c}^3}{{R_H}^3 - {R_c}^3}\right] \tag{2}$$

with R_H and $R_{H,0}$, respectively, the hydrodynamic radius of the core shell at T and at the reference state (45°C). R_c denotes the radius of the core particles determined from the Cryo-TEM. The Flory interaction parameter χ is given by

$$\chi = \frac{\Delta F}{k_b T} = \frac{\Delta H - T\Delta S}{k_b T} = \frac{1}{2} - A\left(1 - \frac{\Theta}{T}\right) \tag{3}$$

where $A = (2\Delta S + k_B)/2k_B$ and $\Theta = 2\Delta H/(2\Delta S + k_B)$. ΔS and ΔH are the changes in entropy and enthalpy of the process, respectively. It has been shown that χ increases nonlinearly with increasing concentration of polymer (see, e.g., [41] and further literature cited therein)

$$\chi(T, \phi) = \chi_1(T) + \chi_2\phi + \chi_3\phi^2 + \ldots \tag{4}$$

with χ_1 corresponding to Eq. 3. Following [15], we will only consider the first order of the ϕ expansion, which leads to the following expression for χ

$$\chi = \frac{\Delta F}{k_b T} = \frac{1}{2} - A\left(1 - \frac{\Theta}{T}\right) + \chi_2\phi \tag{5}$$

Thermodynamic equilibrium for the gel is attained when $\Pi = 0$, i.e., if the pressures inside and outside the gel are the same. Combining Eqs. 1 and 5, the equilibrium line in the $T - \phi$ phase diagram is given by

$$T_{\Pi=0} = \frac{A\phi^2\Theta}{-\phi - ln(1-\phi) + \left(A - \frac{1}{2}\right)\phi^2 - \chi_2\phi^3 + \frac{\phi_0}{N_{\mathrm{Gel}}}\left[\frac{1}{2}\left(\frac{\phi}{\phi_0}\right) - \left(\frac{\phi}{\phi_0}\right)^{\frac{1}{3}}\right]} \tag{6}$$

4 Results and discussion

4.1 Synthesis and characterization of the particles

The synthesis of the core-shell particles proceeds in two steps [31]: First, a poly(styrene) core is synthesized by conventional emulsion polymerization. The core particles thus obtained are practically monodisperse and well-defined. A radius of 52.0 nm and a polydispersity of 9.4% were derived from the Cryo-TEM micrographs, whereas the DLS gives a value of 55.7 nm between 8 and 45°C [6]. As expected, the radius of the core particles as observed by DLS has no dependence on the temperature.

It needs to be noted that the core particles bear a small number of chemically bound charges on their surface. This is due to the synthesis of the cores, which proceeds through a conventional emulsion polymerization. These charges keep the solution stable even at high temperature. This point is of particular importance for the second step in which the thermosensitive shell is polymerized at 80°C onto these core particles by a seeded emulsion polymerization. For the synthesis of the particles under consideration here, we use the same amount of PNIPAM for all three systems and only vary the degree of cross-linking (see Table 1). The core-shell particles are cleansed by exhaustive ultrafiltration to remove possible traces of free polymer in the suspension [31].

Figure 2 shows the micrographs obtained for different degrees of crosslinking by Cryo-TEM. For this analysis, a suspension of the particles is shock-frozen in liquid ethane [40]. The water is supercooled by this procedure to form a glass and the particles can directly be studied in situ. Figure 2 shows that the core-shell particles are indeed narrowly distributed. The thermosensitive shell is clearly visible in these pictures without using any contrast agent. The shell exhibits regions of higher and lower transmission that can be assigned to the thermal density fluctuations, as well as static inhomogeneities in the network. These fluctuations lead to an additional contribution seen in small-angle X-ray scattering (SAXS) measurements of similar core-shell particles [15, 32, 33]. Both types of spatial inhomogeneities are also present in macroscopic networks and are predicted by theory [14]. Hence, Fig. 2 provides a direct visualization of an important conclusion drawn from previous scattering measurements. Moreover, the present micrographs suggest that these fluctuations lead to a slightly irregular shape that may also be embodied

Table 1 Composition (in *g*) of the different core-shell latexes

	KS1	KS2	KS3
PS-core	39.98	40.00	40.00
PNIPAM	38.00	38.00	38.00
BIS	0.65	1.30	2.59

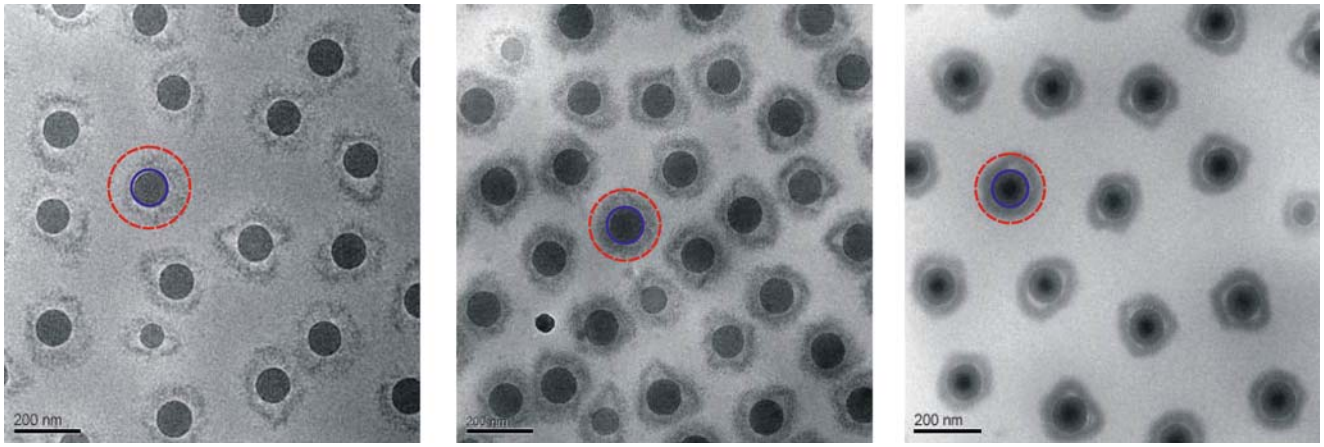

Fig. 2 Cryo-TEM micrographs of a 0.2 wt.% aqueous suspension of the PS/PNIPAM core-shell particles for different degrees of crosslinking: *left*, KS1 1.25 M%; *middle*, KS2 2.5 M%; *right*, KS3 5 M%. The sample was kept at room temperature before vitrification. The core consists of polystyrene and the corona of PNIPAM cross-linked with BIS. The *full* and *dashed lines* show the hydrodynamic radii, respectively, of the core and core-shell particles as determined by DLS

in the contribution to the scattering intensity measured at higher scattering angles. Evidently, this feature is much harder to see in micrographs done by conventional electron microscopy that works in the dry state of the particles [27, 28, 42].

Figure 2 also demonstrates that the thermosensitive shell is, in some cases, not fully attached to the core. There is a buckling of the shell that is decreasing with increasing crosslinking. This buckling of a network affixed to a solid surface has already been found in macroscopic networks and is due to the one-dimensional swelling [43]. Here, we find the same effect for microscopic systems. This result sheds new light on the second step in the synthesis of the core-shell particles: The core particles already have a thin shell of PNIPAM because of the addition of 5% NIPAM during the synthesis of the core particles [31]. The shell will be bound to the core most probably by chain transfer of the growing PNIPAM network to the thin PNIPAM-shell covering the core. At the high temperatures used during the synthesis of the shell, the growing network is collapsed onto the core. Thus, the shell is expected to be rather homogeneous at temperatures above the volume transition. This was shown experimentally by small-angle neutron scattering (SANS) [32] and by Cryo-TEM, indeed [40]. The micrographs demonstrate, however, that the binding is incomplete. Chain transfer does not lead to complete attachment of the shell to the cores in this step. Hence, the three-dimensional swelling of the shell below the transition must lead to a partial detachment of the shells and to the buckling of the shells also at the interface core-shell.

Figure 2 demonstrates that the buckling is decreasing with increasing degree of cross-linking, as expected. Obviously, the affixing of the shell to the core particles is directly related to the amount of crosslinker present in the present stage of the polymerization. This result corroborates recent SANS analysis performed on core-shell consisting of PNIPAM in the shell and poly-*N*-isopropylmethacrylamide in the core also synthesized in a seed emulsion polymerization, which pointed out the presence of a depletion zone at the interface core-shell [30]. Cryo-TEM hence allows us to directly visualize an important aspect of the synthesis of the particles not available by any other method so far.

The volume transition within the shell can easily be studied by DLS. Figure 3 shows the microgel particles radius determined by DLS as a function of the temperature. R decreases gradually with temperature until a sharp volume transition from swollen to the collapsed state takes place. The final size is reached at a transition temperature between 307 and 311 K, depending on the degree of crosslinking. Increasing the degree of crosslinking, the transition becomes more continuous and the collapse state is shifted to higher temperatures. Without the addition of salt, this process is thermoreversible without any hysteresis.

The addition of 5.10^{-2} mol L^{-1} KCl leads to a slight shrinking of the particles. This phenomenon has already been investigated in a recent study [44]. The addition of salt screens the residual electrostatic interaction of the particles. Hence, at higher temperatures, the dispersions become unstable and aggregate [6, 44]. For the systems under consideration, here aggregation takes place above 32°C for the KS1 and about 33°C for the KS2 and KS3. Hence, the residual electrostatic repulsion of the particles that is due to the small number of charges on the cores (see above) can be

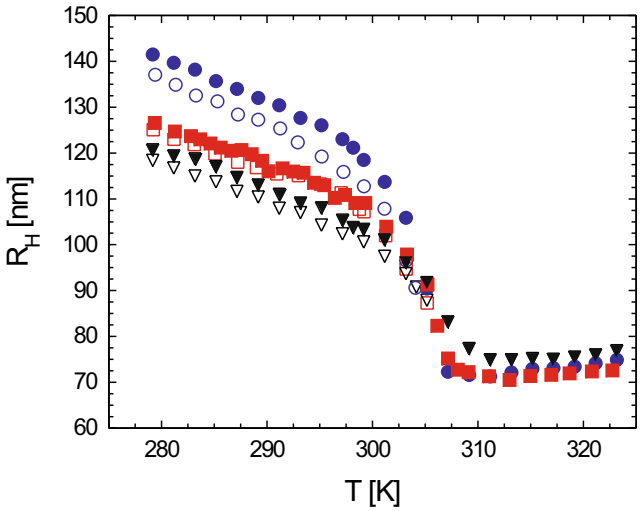

Fig. 3 Hydrodynamic radii of the core-shell latexes vs temperature for different degrees of crosslinking, as determined by DLS (*circles*: 1.25 M%, *triangles*: 2.5 M%, *squares*: 5 M%). *Full symbols* represent the measurements without the addition of salt, whereas *hollow symbols* display the measurements performed by adding 5.10^{-2} mol L^{-1} KCl

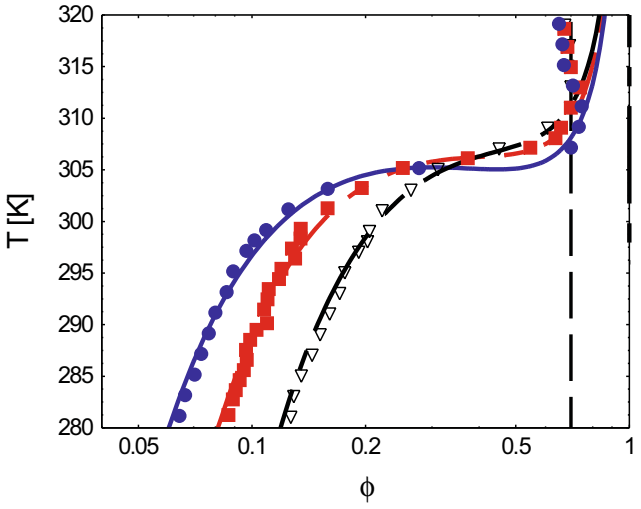

Fig. 4 Experimental phase diagram $T - \phi$ for different degrees of crosslinkings (*full circles*: 1.25 M%, *hollow triangles*: 2.5 M%, *full squares*: 5 M%). *Lines* present the fits obtained from Eq. 6. The volume fractions ϕ of the polymer in the network have been calculated using Eq. 2. The *vertical dashed line* marks the reference volume fraction $\phi_0 = 0.7$ in the collapsed state

switched off easily by the addition of a small amount of salt. Figure 3 demonstrates, however, that the other properties of the particles are hardly changed. Thus, the core-shell particles under consideration can be turned from Yukawa systems to hard spheres.

The comparison between the overall size observed from the micrographs and the hydrodynamic radius, as determined by the DLS, can be observed in Fig. 2. The hydrodynamic radius R_H as measured by DLS is indicated in each case as a red circle around one particle. Evidently, R_H provides an appropriate measure of the average radius of the particles. This fact is of great importance when determining the effective volume fraction of the particles in a concentrated suspension [6].

4.2 Thermodynamics of the phase transition

In this section, we discuss the modeling of the swelling data shown in Fig. 3 in terms of the Flory–Rehner theory [15]. The volume fractions ϕ of the polymer in the network has been calculated using Eq. 2. A parameter of the different sets of data is the degree of crosslinking. Here, the data deriving only from salt-free systems are used to avoid possible problems due to coagulation above the volume transition. The fits are presented in the $T - \phi$ diagram Fig. 4. The resultant fitting parameters are summarized in the Table 2. Since only the amount of crosslinker is changing, the same value for ϕ_0, A, and χ_2 is used for all the systems and only θ and N are varied.

For the present system, the best agreement for the reference polymer volume fraction in the collapsed state has been found for $\phi_0 = 0.7$. This value has already been expected from the previous analysis of the particles by SANS and Cryo-TEM [6]. Also, as reported by recent nuclear magnetic resonance measurements, water molecules are still present in the shell above the lower critical solution temperature (LCST), but they are strongly confined [26].

The N values (see Table 2) found are proportional to the degree of crosslinking but are about two times larger than the ones corresponding to the crosslinking in a homogeneous network. A content of 2.5 M% of the crosslinker BIS would correspond to $N_{\mathrm{gel}} = 20$. This discrepancy can be traced back to the inhomogeneities in the PNIPAM microgels. Indeed, Wu et al. [45] investigated the polymerization of NIPAM and BIS during the microgel synthesis. The crosslinker was found to be consumed faster than the NIPAM, indicating that the

Table 2 Parameters of the Flory–Rehner fit (Eq. 6 and Fig. 4)

	KS1	KS2	KS3
n(BIS)/n(NiPAM) [mol%]	1.25	2.50	5.00
ϕ_0	0.7	0.7	0.7
A	−8.7	−8.7	−8.7
χ_2	0.9	0.9	0.9
Θ [K]	312	314	316
N_{Gel}	80	45	22
LCST [°C]	32.0	33.1	33.7

particles are unlikely to have a uniform composition. This finding has been confirmed by SAXS and SANS, revealing that the segment density in the swollen state is not homogeneous but gradually decays at the surface [29, 32]. Moreover, a high-sensitive calorimetric study has confirmed this finding [21]. However, the present fits provide an excellent description of the data. Thus, the Flory–Rehner approach gives a valid description even of the present microscopic systems within the limits of error.

Figure 5 presents the relation between the temperature and χ obtained from the combination of Eqs. 5 and 6. The LCST was determined by the condition $\chi = 0.5$. We found that increasing the cross-linking shifts the LCST to higher temperature, whereas for 1.25 M% crosslinker, a value of 32°C is found. This corresponds exactly to the LCST of linear PNIPAM chains that was found, confirming former investigations [21]. This again demonstrates that the core-shell microgels can be modeled much in a way of macroscopic systems.

4.3 Crystallization

The crystallization of pure NIPAM microgels has already been investigated intensively [24, 28, 46, 47]. Here, the crystallization of the samples has been investigated after screening of the electrostatic interactions by adding $5{\cdot}10^{-2}$ mol L^{-1}. We find that all samples crystallize at defined concentrations despite the slightly irregular shape. Obviously, the fluctuations of the network in the shell have no impact on the stability of the crystalline phase. Moreover, the polydispersity of the particles is small [6].

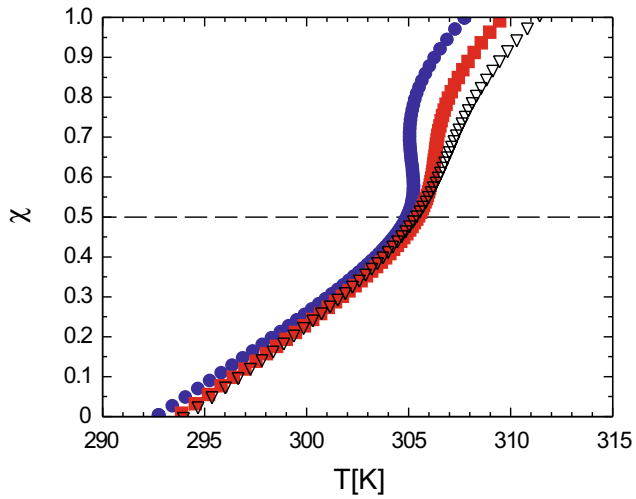

Fig. 5 Solvent parameter χ as determined from the fits of Fig. 4 for different degrees of crosslinking (*full circles*: 1.25 M%, *hollow triangles*: 2.5 M%, *full squares*: 5 M%). Decreasing the degree of crosslinking, the PNIPAM network shrinks upon heating from a continuous to a discontinuous fashion to reach a collapsed state for $\chi = 1$. $\chi = 0.5$ is indicated by the *dashed line* and lays approximately at 32°C, which corresponds to the LCST of pure PNIPAM in aqueous solution

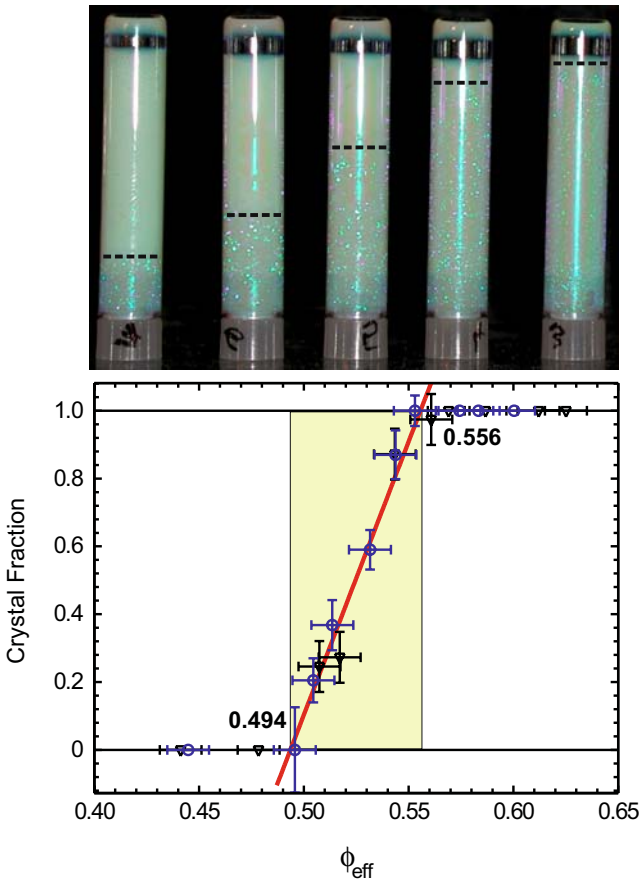

Fig. 6 Core-shell suspension with 5 mol% crosslinking at 20.5°C after 2 months in the biphasic region (*above*) and the corresponding experimental phase diagram (*below*). The crystal fraction determined from the height of the coexistence boundaries has been fitted by a linear regression (*solid line*) for the KS2 (*hollow triangles*) and the KS3 (*hollow circles*). The data have been rescaled to ϕ_F=0.494 to compare to the hard spheres diagram (*long dashed line*)

As already discussed in [6], the effective volume fraction ϕ_{eff} of the particles can be derived from DLS. The hydrodynamic radius of the microgel R_H leads to ϕ_{eff} of the particles in suspension by

$$\phi_{\text{eff}} = \phi_c \left(\frac{R_H}{R} \right)^3 \tag{7}$$

where R is the core radius calculated from the Cryo-TEM and ϕ_c is the volume fraction of the cores in the system. The latter quantity can be approximated from the weight concentration of the particles in the system and the mass ratio of poly(styrene) in the particles.

The established liquid–crystal coexistence domain for hard spheres lays between the freezing volume frac-

tion ϕ_F at $\phi_{\text{eff}} = 0.494$ and the melting volume fraction ϕ_M at $\phi_{\text{eff}} = 0.545$ as obtained from computer simulation [48]. An experimental phase diagram could be achieved by determining the crystal fraction of the samples from the position of the coexistence liquid–crystal boundaries after sedimentation. This can be linearly extrapolated to determine the beginning and the end of the coexistence domain [49, 50]. Figure 6 exhibits the different samples in the liquid–crystalline region and the corresponding rescaled phase diagram. The experimental phase diagram of the KS2 was taken from a previous study [6]. The samples KS1 and KS3 were shaken after preparation to destroy residual crystallites and stored for more than 1 month at room temperature 20.5 ± 0.5°C. After this time, the crystals seen through the Bragg reflections have sedimented for the two highest degrees of cross-linking. For the KS1, the crystals have not sedimented under these conditions but the coexistence domain is manifested by the presence of distinct crystals for effective volume between 0.470 and 0.567. The experimental phase diagram was taken from the change in the position of the coexistence boundary has been observed after 1 month [6]. As expected, the experimental points exhibit a linear dependence in the biphasic region. To compare the two experimental phase diagrams obtained for KS2 and KS3, the data have been rescaled to $\phi = 0.494$. The rescaled coexistence domain has been found between 0.494 and 0.556. This is more or less in accord with the theoretical values $\phi_M = 0.545$ [48].

This good agreement of the experimental phase diagram of the core-shell particles with the prediction for hard spheres demonstrates that the particles can be treated as hard spheres at least up to a volume fraction of 0.55. This result is very important for the use of these suspension as model systems for rheological experiments [6].

5 Conclusion

Composite PS/PNIPAM core-shell microgels with different degrees of crosslinking have been synthesized and analyzed by Cryo-TEM and DLS. The crosslinked PNIPAM-shell forms a well-defined network around the practically monodisperse core particles. Direct imaging of the particles by Cryo-TEM shows the inhomogeneities within the network. Cryo-TEM also shows the buckling of the shell caused by the one-dimensional swelling of the shell. This buckling effect, which is well-known from macroscopic systems, leads to a slightly irregular shape of the particles. The volume transition within the shell of these particles can be described very well by the Flory–Rehner theory. The polydispersity of the outer radius of the particles is small and the particles crystallize at effective volume fractions predicted for a suspension of hard spheres. All results demonstrate that the two-step synthesis of the particles leads to well-defined particles suitable as model systems for studying the dynamics of concentrated suspensions.

References

1. Suzuki A, Tanaka T (1990) Nature 346:345
2. Ilmain F, Tanaka T, Kokufuta E (1991) Nature 349:400
3. Hirotsu S (1994) Phase Transit 47:183
4. Nayak S, Lyon LA (2005) Angew Chem Int Ed 44:7686
5. Anderson VJ, Lekkerkerker HNW (2002) Nature 416:811
6. Crassous JJ, Siebenbürger M, Ballauff M, Drechsler M, Henrich O, Fuchs M (2006) J Chem Phys 125:204906
7. Taniguchi T, Duracher D, Delair T, Elaïssari A, Pichot C (2003) Colloid Surf B Biointerfaces 29:53
8. Duracher D, Veyret R, Elaïssari A (2004) Polym Int 53:618
9. Lu Y, Mei Y, Drechsler M, Ballauff M (2006) Angew Chem Int Ed 45:813
10. Lu Y, Mei Y, Drechsler M, Ballauff M (2006) J Phys Chem B 10:10
11. Tanaka T, Sato E, Hirakawo Y, Hirotsu S, Peetermans J (1985) Phys Rev Lett 55:2455
12. Shibayama M, Tanaka T, Han C (1992) J Chem Phys 97:6829
13. Shibayama M, Tanaka T (1993) Adv Polym Sci 109:1
14. Shibayama M (1998) Macromol Chem Phys 199:1
15. Fernández-Barbero A, Fernandez-Nieves A, Grillo I, López-Cabarcos E (2002) Phys Rev E 66:051803
16. Flory PJ (1953) Principles of polymer chemistry. Cornell University Press, Ithaca
17. Huggins ML (1964) J Am Chem Soc 86:3535
18. Flory PJ (1970) Discuss Faraday Soc 49:7
19. Baulin VA, Halperin A (2003) Macromol Theory Simul 12:549
20. Schild HG, Tirrell DA (1990) J Phys Chem 94:4352
21. Woodward NC, Chowdhry BZ, Snowden MJ, Leharne SA, Griffiths PC, Winnington AL (2003) Langmuir 19:3202
22. Andersson M, Hietala S, Tenhu H, Maunu SL (2006) Colloid Polym Sci 284:1255
23. Hoare T, Pelton R (2007) J Phys Chem B 111:1334
24. Senff H, Richtering W (1999) J Chem Phys 111:1705
25. Senff H, Richtering W, Norhausen C, Weiss A, Ballauff M (1999) Langmuir 15:102
26. Sierra-Martin B, Choi Y, Romero-Cano MS, Cosgrove T, Vincent B, Fernandez-Barbero A (2005) Macromolecules 38:10782
27. Makino K, Yamamoto S, Fujimoto K, Kawaguchi H, Oshima H (1994) J Colloid Interface Sci 166:251
28. Hellweg T, Dewhurst CD, Eimer W, Kratz K (2004) Langmuir 20:4330
29. Stieger M, Richtering W, Pedersen JS, Linder P (2004) J Chem Phys 120:6197
30. Berndt I, Pedersen JS, Richtering W (2006) Angew Chem Int Ed 45:1737
31. Dingenouts N, Norhausen Ch, Ballauff M (1998) Macromolecules 31:8912
32. Seelenmeyer S, Deike I, Rosenfeldt S, Norhausen Ch, Dingenouts N, Ballauff M, Narayanan T (2001) J Chem Phys 114:10471

33. Dingenouts N, Seelenmeyer S, Deike I, Rosenfeldt S, Ballauff M, Lindner P, Narayanan T (2001) Phys Chem Chem Phys 3:1169
34. Ballauff M, Lu Y (2007) Polymer 48:1815
35. Crassous JJ, Regisser R, Ballauff M, Willenbacher N (2005) J Rheol 49:851
36. Fuchs M, Ballauff M (2005) J Chem Phys 122:094707
37. Fuchs M, Cates ME (2002) Phys Rev Lett 89:248304
38. Fuchs M (2003) Faraday Discuss 123:267
39. Fuchs M, Ballauff M (2005) Colloids Surf A 270-271:232-8
40. Crassous JJ, Ballauff M, Drechsler M, Schmidt J, Talmon Y (2006) Langmuir 22:2403
41. Eichinger BE, Flory PJ (1968) Trans Faraday Soc 64:2275
42. Ziesmer S, Stock N (2008) Colloid Polym Sci in press
43. Boudaoud A, Chaïeb S (2003) Phys Rev E 68:021801
44. Lopez-Leon T, Ortega-Vinuesa JL, Bastos-Gonzalez D, Elaïssari A (2006) J Phys Chem B 110:4629
45. Wu X, Pelton RH, Hamielec AE, Woods DR, McPhee W (1994) Colloid Polym Sci 272:467
46. Tang SJ, Hu ZB, Cheng ZD, Wu JZ (2004) Langmuir 20:8858
47. Lyon LA, Debord JD, Debord SB, Jones CD, McGrath JG, Serpe MJ (2004) J Phys Chem B 108:19099
48. Hoover WG, Gray SG, Johnson KW (1971) J Chem Phys 55:1128
49. Pusey PN, van Megen W (1986) Nature 320:340
50. Paulin SE, Ackerson BJ (1990) Phys Rev Lett 64:2663